Supplementary Materials for

Apatite ^{4}He/^{3}He and (U-Th)/He Evidence for an Ancient Grand Canyon

R. M. Flowers* and K. A. Farley

*To whom correspondence should be addressed. E-mail: rebecca.flowers@colorado.edu

This PDF file includes:

Materials and Methods
Figs. S1 to S3
Full Reference List

Other Supplementary Material for this manuscript includes the following:
(available at www.sciencemag.org/cgi/content/full/science.1229390/DC1)

Tables S1 to S6 (in an Excel file)

Materials and Methods

<u>Experimental work</u>

All samples analyzed here were described and dated previously with the (U-Th)/He method (*23, 26*) (Table S1). AHe data for GC863 are reported in full here for the first time (Table S6), although they were discussed previously (*26*). Preliminary versions of four of the ^{4}He/^{3}He spectra for sample GC863 were plotted previously (*26*), but the remaining ^{4}He/^{3}He data have not been presented before (Table S1, S2).

Apatites were irradiated for the production of uniformly-distributed spallogenic ^{3}He in several different batches at the Francis H. Burr Proton Therapy Center, following procedures outlined previously (*33*). Individual crystals for ^{4}He/^{3}He analysis were selected on the basis of large size and full euhedral morphology, measured for the α ejection correction (*34*), loaded into small Pt tubes, placed in a copper foil sheath and mounted on a thermocouple wire in a projector lamp diffusion cell (*35*). Helium was accumulated at temperatures between 200 and 500°C for between 0.25 and 4 hours, purified over SAES getters, and measured on the electron multiplier spur of a GV-SFT mass spectrometer in peak-hopping mode. The final step for each sample (and for some samples multiple such steps) was performed by laser-heating of the Pt package after transfer to an appropriate chamber. An empty tube was used to measure temperature-dependent blanks. Tabulated data are corrected for these blanks, which averaged 0.3 pcc of He with ^{4}He/^{3}He~1000. Stated uncertainty includes a 50% uncertainty in the blank correction as well as a signal-size dependent uncertainty based on the external precision of standards of similar count rate.

^{4}He/^{3}He spectra were computed from blank-corrected peak heights and "bulk-normalized" to the total ^{4}He and ^{3}He obtained from the sample (*36*). All data points were included in this computational step.

^{4}He/^{3}He spectra were converted to normalized ^{4}He/^{3}He age spectra (*36*) using measured grain dimensions and the appropriate α-ejection-only ^{4}He/^{3}He spectrum. Table S2 reports all ^{4}He/^{3}He data. All normalized ^{4}He/^{3}He age spectra are plotted in Figures 2, 3, and S1. All analyzed apatites except those from sample CP06-Diab had grain terminations morphologically typical for apatite, so we are confident that an entire grain was analyzed. In contrast the majority of grains in sample CP06-Diab had two perpendicular terminations. Thin sections reveal that the apatites in this diabase are unusually elongated, with length/width ratios much greater than in the apatite separate. Thus the perpendicular terminations on the analyzed grains suggest we are working with broken grains. As described previously (*25*), broken grains bias ^{4}He/^{3}He spectra and therefore we must make a correction for this effect before interpreting the results.

We adopted the following procedure to correct sample CP06-Diab (only) for breakage. This method is based on modeling described previously (*25*). We assume that one or both terminations were originally located well to the interior of the original termination(s), such that there is no ejection or diffusion rounding of the ^{4}He profile at the observed termination. The broken terminations constitute a fraction (1-x) of the surface area of the sample, with a fraction x associated with the sides of the cylinder. In this situation, the normalized ^{4}He/^{3}He ratio for a given step in the spectrum is approximately (*25*):

$$R_m \approx xR_s + (1 - x) \times 1$$

where R_m is the measured bulk-normalized $^4He/^3He$ ratio, R_s is the bulk-normalized $^4He/^3He$ ratio being degassed from the sides of the cylinder (and any unbroken terminations), and the factor of 1at the end of the expression is the approximate normalized $^4He/^3He$ ratio degassing out of the broken terminations.

The normalized $^4He/^3He$ age spectrum is obtained by dividing R_m by R_a (the α-ejection only profile (*36*)) for each step. Thus for an apatite with broken termination(s):

$$\frac{R_m}{R_a} \approx x\frac{R_s}{R_a} + \frac{(1 - x)}{R_a}$$

As discussed below we use HeFTy *(37)* to model the normalized age spectrum R_s/R_a. So, we can rearrange the expression above to yield the desired quantity:

$$\frac{R_s}{R_a} \approx \frac{\frac{R_m}{R_a}}{x} - \frac{(1 - x)}{xR_a}$$

In this expression the quantity R_m is measured for a given step and R_a is computed from an α-ejection-only profile subjected to the same extent of degassing as the measured step (*36*). x is computed from grain geometry assuming a right cylinder with either 1 or 2 broken terminations, depending on observations. Results of these corrections are listed in Table S2; the corrections were assumed to add an additional uncertainty of ±10% to each step of the $^4He/^3He$ spectrum.

Table S2 lists all of the $^4He/^3He$ spectra we obtained on apatites from Grand Canyon. Several of these spectra have such large uncertainties as to be unusable (e.g., CP06-Bass (c)). Others have single or multiple steps that deviate from any conceivable diffusion-produced profile (e.g., CP06-Diab (TCPb) and CP06-69 (b)) for presently unknown but probably analytical reasons. Rather than reject these steps and retain the spectrum we instead reject the entire spectrum from further consideration. Thus the normalized age spectra shown in the main text are those with both reasonably high analytical precision and consistent with a diffusion process. Attempts to include the aberrant spectra in our inversion model would have led to rejection of all conceivable time-temperature paths, obviously a non-physical result.

Zonation in U and Th were measured on at least four different grains of each sample using laser-ablation ICPMS following previously reported procedures (*26*). A summary of the zonation data is provided in Table S3. The complete individual profile data are reported in Table S4. Figure S2 shows the zonation profiles for all samples.

Time-Temperature Modeling
Overview

HeFTy (*37*) is a software tool for computing He dates and $^4He/^3He$ spectra on arbitrary time-temperature paths given a He diffusion kinetic model and a map of the grain's eU distribution. It assumes spherical symmetry in all quantities. We used this program to generate a large population of time-temperature paths on which were simultaneously simulated AHe dates and age spectra for a data ensemble associated with samples from a specific locality (e.g., those from western Grand Canyon). The data ensemble includes both bulk date and $^4He/^3He$ spectra constraints. We chose reasonable values for grain size, eU, and zonation pattern for each of the simulated samples as described below and summarized in Table S5. We used the RDAAM kinetic model

because it includes the most recent understanding of the role of radiation damage (and its annealing) on He diffusivity (28). The HeFTy implementation of the RDAAM model incorporates spatial and temporal variability in He diffusion coefficients arising from variations in the amount of radiation damage accumulated at a given radial location in the grain. Because HeFTy does not yet perform inverse modeling that includes ^{4}He/^{3}He spectra, we exported the results for each tested time-temperature path for further analysis as discussed below.

The goal of this effort is to falsify with a given statistical certainty the hypothesis that a given time-temperature path yields results that are consistent with observations. Falsified paths can be rejected, leaving as survivors only paths that are consistent with the data. To the extent that the entire space of reasonable paths has been investigated, the survivors constrain the allowed cooling path experienced by the locality from which the ensemble was sampled. Of course this approach implicitly assumes that the underlying kinetic model used in the computations is valid.

Comparison for a Single Observation
1) Date

We used HeFTy's (37, 38) (version 1.7.4) goodness-of-fit criterion (G) to evaluate how well the date modeled on a tested path agrees with the measured date of each sample given the stated measurement uncertainty. The null hypothesis to be evaluated is that the measured and modeled date are different, and the G parameter indicates the probability that the null hypothesis can be rejected. Thus low values of G indicate a poor match to the measured date, and a low probability that the null hypothesis can be rejected. Similarly high values of G indicate a good match to the measured date and a high probability that the null hypothesis can be rejected. By selecting an appropriate threshold value for G, paths that do not meet the date criterion with a confidence level G are rejected. The G values we adopted in our modeling are listed in Table S5.
2) ^{4}He/^{3}He spectra

We chose to use the normalized age spectrum as the fitting target for our modeling. This spectrum is more readily compared with models than the normalized ^{4}He/^{3}He spectrum because it eliminates the (path-independent) effects of α ejection (36). In addition this spectrum is independent of the bulk date of the sample (unlike the ^{4}He/^{3}He age spectrum), which allows us to independently evaluate the fit to the bulk date and to the spectrum itself.

For every time-temperature path we tested, we simulated the normalized age spectrum relevant to a specific sample in terms of grain size, eU, zonation, etc. We then compared this simulated spectrum to the one measured on the associated sample. The first step in this comparison is to linearly interpolate the simulated spectrum to the same steps in ΣF^3He as in the measured data so that each step can be directly compared. The total mismatch E_{S-M} between the interpolated simulation and the measured spectrum is:

$$E_{S-M} = \Sigma_1^n \left| A_i^S - A_i^M \right|$$

where n is the number of steps, A_i is the normalized age of step i, and superscripts S and M indicate simulated and measured values, respectively. In this computation we excluded the few steps indicated in Table S2 with yields less than 0.5% since they are very uncertain. We also observed that rare data points lie well outside reasonable bounds, suggesting a presently unknown and erratic source of error. To avoid having a few steps

dominate the mismatch, for each measured spectrum we excluded the single data point with the largest mismatch from the computation.

We seek to compare E_{S-M} to the mismatch that would arise solely from experimental uncertainties added to an otherwise perfect match to the test spectrum. We used a Monte-Carlo approach; for each simulated age spectrum, we generated 25,000 realizations of the simulated spectrum by adding to each step a quantity D. D was chosen from a bidirectional Gaussian distribution with width taken from the absolute uncertainty on that specific step. For example, if a given step of a particular target spectrum has an experimental uncertainty of ±0.1, then D was drawn from a Gaussian distribution with a mean of zero and a standard deviation of 0.1. For each of these realizations (indicated by subscript r) we computed the total mismatch with the original (error-free) simulated model:

$$E_{S-r} = \Sigma_1^n \left| A_i^S - \left(A_i^S + D \right) \right|$$

From the 25,000 realizations we obtain a statistical portrait of the consequences of the experimental uncertainty on the magnitude of mismatch arising solely from experimental uncertainty. By comparing the observed mismatch E_{S-M} with this portrait we obtain a statistical measure of the probability that the mismatch exceeds random analytical error added to an underlying perfect fit. Again we use the goodness of fit parameter G to evaluate the null hypothesis that the modeled spectrum is distinct from the measured spectrum given measurement uncertainties, and G is the probability that the null hypothesis can be rejected. For example, if the observed mismatch E_{S-M} exceeds all but 5% of the E_{S-r} values in the statistical portrait, then G=0.05 (low probability that the null hypothesis can be rejected). Similarly if E_{S-M} is smaller than 95% of the E_{S-r} values, then G=0.95 (high probability that the null hypothesis can be rejected). By selecting an appropriate threshold value for G, paths that do not meet the ^{4}He/^{3}He spectrum criterion with a confidence level G can be rejected. The remaining paths are considered survivors statistically consistent with this particular observation.

Paths that Satisfy the Ensemble of Observations

Our computation generates a family of surviving paths for each individual observation. The surviving paths that satisfy the entire data ensemble are those (and only those) that survive all of the individual constraints.

Details of Specific Inverse Models

Inverse model constraints for both eastern and western Grand Canyon simulations included bulk AHe data for four samples and multiple apatite ^{4}He/^{3}He normalized age spectra. The ensemble of constraints used in each simulation is listed in Table S5. The sample mean AHe date, mean apatite eU, and mean equivalent spherical radius (r) were defined, and a representative apatite eU zonation profile was assumed, for each dated sample. The exception was GC863, for which no zonation was assumed because the mean F_{TZ}/F_{TH} value for the apatites from this sample was near 1 despite the extreme zonation heterogeneity (*26*). For the apatite ^{4}He/^{3}He constraints, the same representative eU zonation profile and mean eU value was applied as for the AHe constraint, with r values in the same range as the apatites analyzed by ^{4}He/^{3}He from the sample.

For eastern Grand Canyon samples, we applied peak temperatures constraints of 120-110 °C from 85-80 Ma. Apatite-fission track data suggest complete apatite annealing

and peak temperatures of >110 °C; the exact choice of peak temperature does not impact our results. Cretaceous units preserved in the Black Mesa Basin (39) in northeastern Arizona only 80-100 km away from eastern Grand Canyon indicate that deposition continued until at least 85 Ma, consistent with peak burial temperature attainment by ~80 Ma. For western Grand Canyon samples, we loosened the bound on when peak temperatures were attained to 100-80 Ma, owing to the older AHe dates here and the more distal location from the Black Mesa Basin constraint. In all cases we assumed surface temperatures of 25-20 °C (see below).

For all inverse simulations we assumed an episodic cooling history, with each segment between the constraints consisting of 6 to 8 randomly defined linear segments. Goodness of fit thresholds of G=0.3 for AHe dates and G=0.15 for ^{4}He/^{3}He spectra were used to define statistically acceptable paths in eastern Grand Canyon. For western Grand Canyon, thresholds of G=0.3 for AHe dates and G=0.32 for ^{4}He/^{3}He spectra were imposed.

Details of Specific Forward Models

We carried out a suite of forward models to predict AHe dates and apatite ^{4}He/^{3}He spectra for western Grand Canyon using the best-fit thermal history from the inverse modeling simulations (Fig. 3C, red path) and a thermal history representative of the "young" post-6 Ma canyon incision model (Fig. 3C, blue path). We derived the latter from the incision history proposed in ref. (4), which depicts 12 longitudinal profiles through the canyon at different times from 6 Ma to the present. Specifically, we constructed this "young" canyon model as follows: 1) We assumed an initial phase of cooling occurred between 90 and 75 Ma, in the same time frame but of lesser magnitude than the cooling phase in the ancient canyon model derived from the inverse modeling simulations, so that we could isolate the influence of the post-75 Ma thermal history on the ^{4}He/^{3}He spectra. 2) The model of ref. (4) shows ~725 m of incision in western Grand Canyon between 6 Ma and the present. Assuming a 25 °C/km geotherm and 25 °C surface temperature implies that the rocks exposed in western Grand Canyon today were at temperatures of ~43 °C at 6 Ma. For simplicity we conservatively assume that the rocks had resided at ~43 °C for the entire period between 75 and 6 Ma. Residence at higher temperatures would cause greater He loss from the apatites, and make it even more difficult for the young canyon model to reproduce the He data. 3) The model of ref. (4) depicts ~200 m of incision between 6 and 5 Ma, and another ~200 m between 5 and 4 Ma. Making the same geotherm and surface temperature assumptions above implies an ~5°C reduction of temperature associated with each 200 m of incision, thus reducing temperatures to 38 and 33 °C at 5 and 4 Ma, respectively. 4) The ref. (4) model shows ~165 m of incision between 4 and 2 Ma, and incision of this same magnitude between 2 Ma and the present. Our time-temperature path therefore shows temperature drops of 4 °C over each of these intervals, with temperatures of 29 °C and 25 °C at 2 Ma and the present. Note that the predicted apatite ^{4}He/^{3}He spectra and AHe dates are insensitive to minor variations in the post-6 Ma time-temperature path involving secondary accelerations or decelerations of cooling.

A 25 °C/km paleogeothermal gradient is compatible with Tertiary geotherms calculated in the South Virgin Mountains, located 10-20 km northwest of where the Colorado River exits the western margin of the plateau (21). The assumed modern

surface temperature of 25 °C in the forward models is based on surface temperatures derived from shallow borehole data (*21*). We consider this 25 °C surface temperature assumption for the entire post-70 Ma portion of the history to be a conservative one, because global cooling of climate by 3-8 °C occurred during the late Cenozoic (*40*). However, for completeness, we also tested an alternative cooler endmember young canyon history assuming a 20 °C/km geotherm and 20 °C surface temperature, but otherwise using the same approach for thermal history construction as described above (Fig. S3A). There is little difference between the ^{4}He/^{3}He spectra yielded by this endmember time-temperature path and the reference young canyon thermal history in Figure 3C (blue path).

The RDAAM kinetic model (*28*) was developed and calibrated using a He diffusion kinetic dataset for natural samples (*27*). Four parameters sets were selected for RDAAM that span the range of acceptable fits to the He diffusion data. These parameter sets yield similar results for most investigated thermal histories, and so in this and other studies we employ one of these representative parameter sets. The bottom panel of Figure S3A shows the apatite ^{4}He/^{3}He spectra predicted using the reference young canyon model (Fig. 3C, blue path), but employing the three alternative parameter sets, and demonstrates that the predicted ^{4}He/^{3}He spectra are insensitive to the parameter set choice.

For both the best-fit ancient canyon and young canyon histories, we predicted the AHe dates for all apatite eU zonation profiles acquired for western Grand Canyon samples. We either used the measured mean eU and mean r values of the zonation profiles if they were in the same range as the dated grains, or converted the eU and r values to the mean of the dated sample if outside that range. Because there were many more zonation profiles acquired for GC863 than apatites dated, we plotted a representative subset of these results in the Figure 3A histogram, equivalent to the number of grains dated and plotted in the top histogram panel. The choice of subset plotted does not impact the overall data distribution.

We also predicted the normalized ^{4}He/^{3}He age spectra for the two western Grand Canyon samples with ^{4}He/^{3}He data. We show the predictions for a representative zonation profile from sample CP06-69 in Figure 3B. The predictions for all apatite zonation profiles from CP06-69 and GC863 are shown in Figure S3. For these forward models, we used the mean r value of the apatite zonation profile if it is in the same range as the apatites analyzed for ^{4}He/^{3}He. If the profile is outside this range, we converted it to the mean r value of the apatites for which ^{4}He/^{3}He data were acquired. Although extreme zonation heterogeneity in GC863 apatites prevents a unique comparison of predicted and observed spectra for individual crystals, the overall fit of the data suite from this sample can be assessed. We therefore compare predicted age spectra for the 30 apatite zonation profiles for both the "ancient" and "young" Grand Canyon time-temperature paths with the observed suite of apatite ^{4}He/^{3}He spectra from this sample. The results show that the ^{4}He/^{3}He spectra predicted by the young canyon model are characterized by greater He loss from the outer portions of the grains than observed, and yield a qualitatively poorer fit than the ancient canyon model predictions (Fig. S3B).
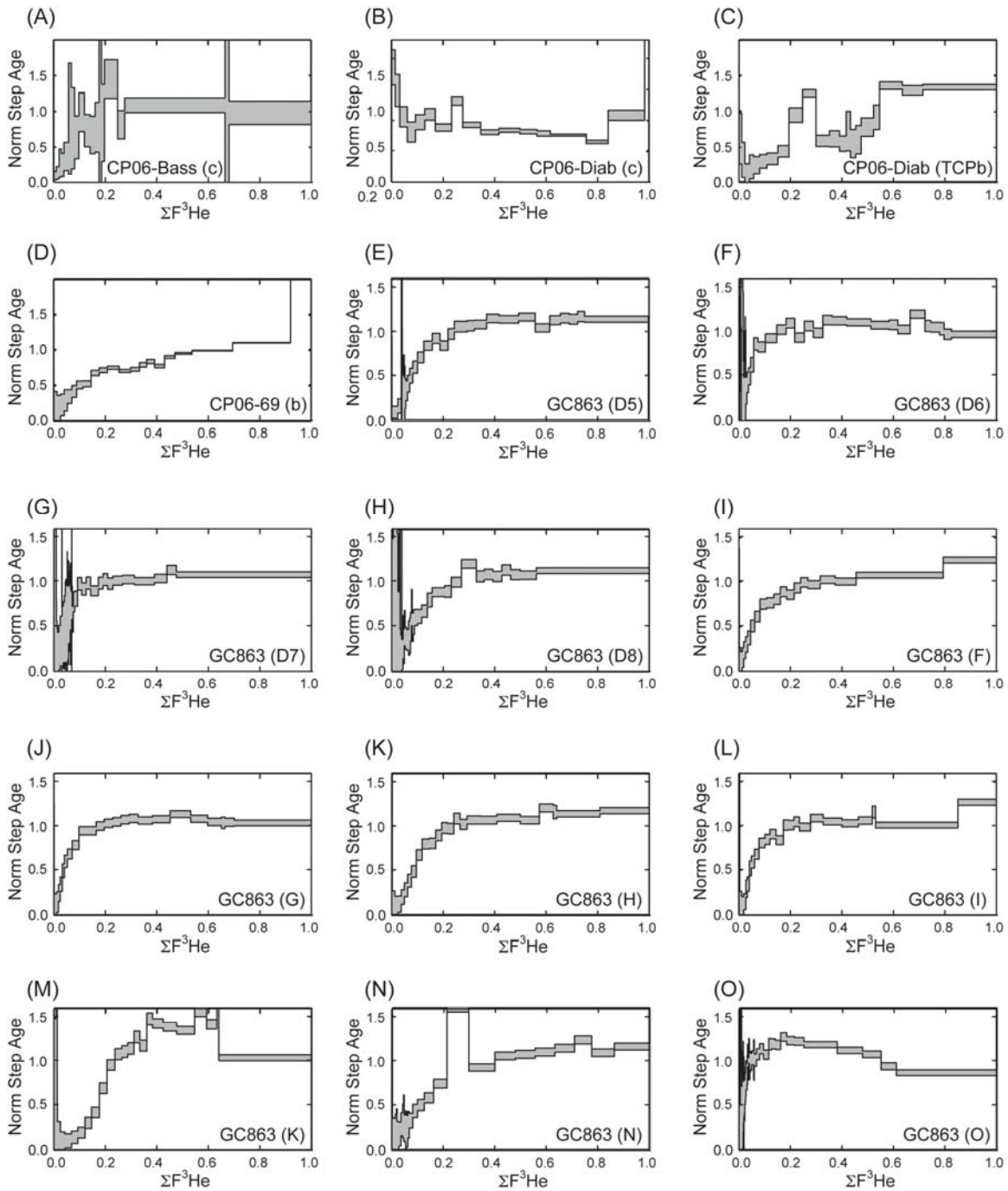
Fig. S1.

Normalized age spectra for apatites not shown in Figures 2 and 3 from (A) CP06-Bass, (B)-(C) CP06-Diab, (D) CP06-69, and (E)-(O) GC863. The patterns shown in panels (A)-(D) are inconsistent with simple diffusion and likely indicate unrecognized analytical or sample problems, and so were rejected from further consideration. The remaining patterns in (E)-(M) occur in a sample in which the apatites are extremely zoned in eU.
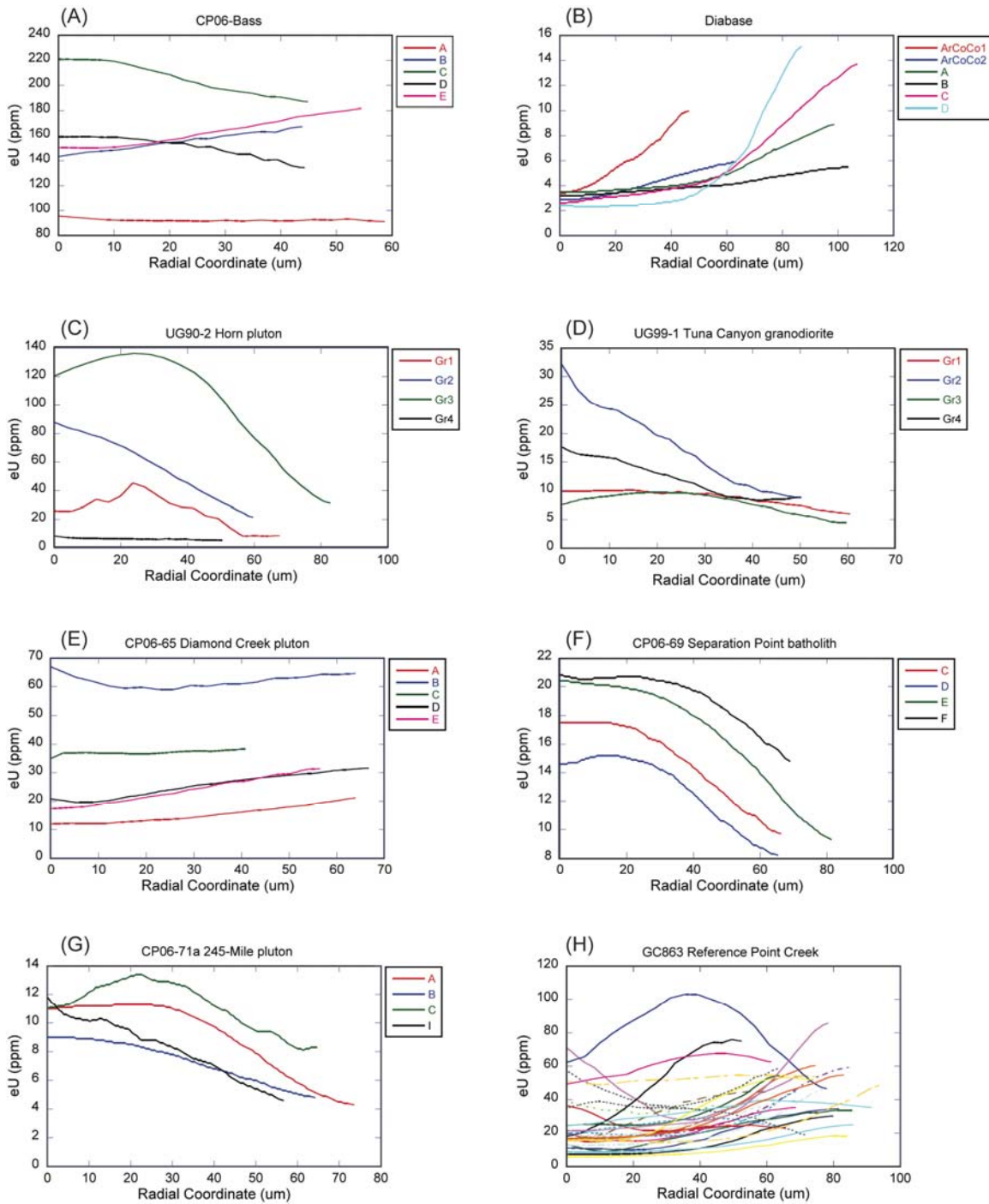
Fig. S2

Apatite eU zonation patterns for canyon-bottom samples from (A)-(D) eastern Grand Canyon and (E)-(H) western Grand Canyon. The apatite center is at radial coordinate = 0. (B) includes data for apatites from two different diabase samples, CP06-Diab and ArCoCo. Refer to (*24*) for additional discussion of GC863 zonation profiles.
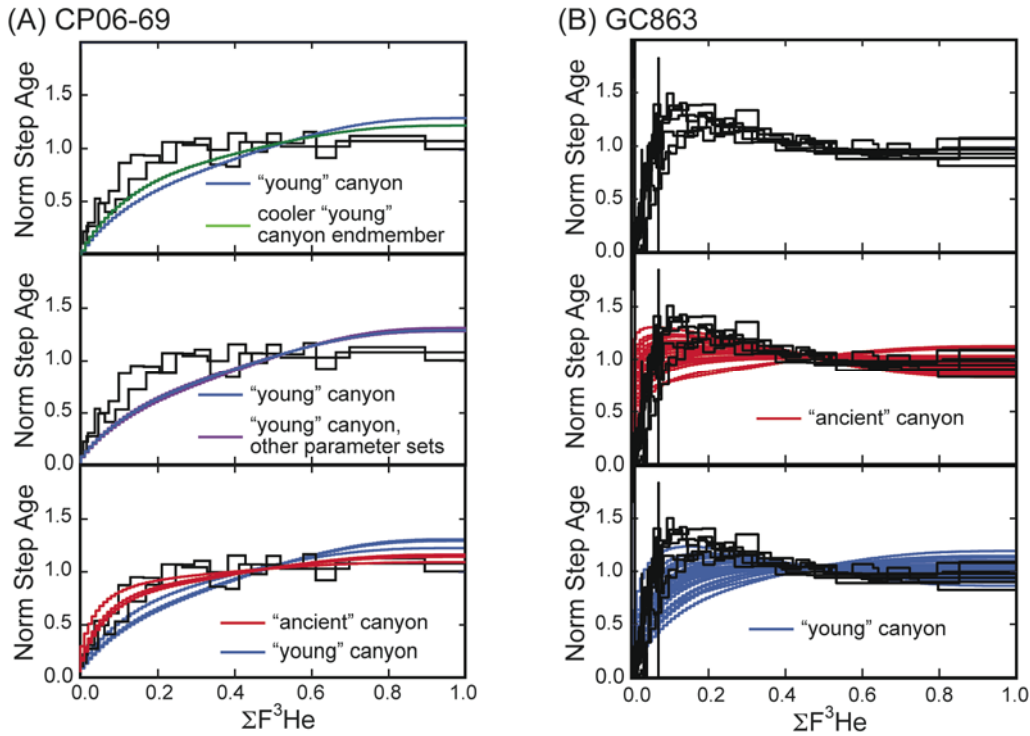
Fig. S3

Forward model predictions for western Grand Canyon. (A) Normalized step age plots for two single-grain apatites from CP06-69 compared with forward model profile predictions for this same sample. Top panel shows that the reference young canyon time-temperature path predicts little difference in the apatite ^{4}He/^{3}He spectra from a time-temperature path that assumes an endmember cooler geotherm and surface temperature. Middle panel demonstrates that utilizing the four different diffusivity parameter sets of the RDAAM model yields no substantive difference in the ^{4}He/^{3}He spectra prediction of the young canyon model. Bottom panel depicts forward model predictions for the four apatites with eU zonation data, and shows that the best-fit ancient canyon model in red yields a better match to the ^{4}He/^{3}He spectra than the prediction of the young canyon model in blue (see thermal histories in Fig. 3D). (B) Normalized step age plots for seven single-grain apatites from GC863. Aberrant data for grains (k) and (n) are excluded. Top panel shows measured age spectra. Normalized age spectra predictions for the 30 apatites with eU zonation data are shown for the best-fit ancient canyon model (middle panel) and the young canyon model (bottom panel).

Table S1.

Sources of data for simulated samples.

Table S2.

Single-grain apatite ^{4}He/^{3}He data.

Table S3.

Apatite eU zonation data summary.

Table S4.

Apatite eU zonation data.

Table S5.

Inverse modeling ensembles.

Table S6.

Apatite (U-Th)/He data for GC863.

References and Notes

1. E. Blackwelder, Origin of the Colorado River. *Geol. Soc. Am. Bull.* **45**, 551 (1934).

2. C. R. Longwell, How old is the Colorado River? *Am. J. Sci.* **244**, 817 (1946). doi:10.2475/ajs.244.12.817

3. I. Lucchitta, Early history of the Colorado River in the Basin and Range Province. *Geol. Soc. Am. Bull.* **83**, 1933 (1972). doi:10.1130/0016-7606(1972)83[1933:EHOTCR]2.0.CO;2

4. K. E. Karlstrom, R. Crow, L. J. Crossey, D. Coblentz, J. W. Van Wijk, Model for tectonically driven incision of the younger than 6 Ma Grand Canyon. *Geology* **36**, 835 (2008). doi:10.1130/G25032A.1

5. J. L. Pederson, The mystery of the pre–Grand Canyon Colorado River—Results from the Muddy Creek Formation. *GSA Today* **18**, 4 (2008). doi:10.1130/GSAT01803A.1

6. J. E. Spencer, P. A. Pearthree, in *Colorado River Origin and Evolution*, R. A. Young, E. E. Spamer, Eds. (Grand Canyon Association, Grand Canyon, AZ, 2001), pp. 215–222.

7. I. Lucchitta, R. F. Holm, B. K. Lucchitta, A Miocene river in northern Arizona and its implications for the Colorado River and Grand Canyon. *GSA Today* **21**, 4 (2011). doi:10.1130/G119A.1

8. K. E. Karlstrom *et al*., ^{40}Ar/^{39}Ar and field studies of Quaternary basalts in Grand Canyon and model for carving Grand Canyon: Quantifying the interaction of river incision and normal faulting across the western edge of the Colorado Plateau. *Geol. Soc. Am. Bull.* **119**, 1283 (2007). doi:10.1130/0016-7606(2007)119[1283:AAFSOQ]2.0.CO;2

9. J. Pederson, K. Karlstrom, W. Sharp, W. McIntosh, Differential incision of the Grand Canyon related to Quaternary faulting—Constraints from U-series and Ar/Ar dating. *Geology* **30**, 739 (2002). doi:10.1130/0091-7613(2002)030<0739:DIOTGC>2.0.CO;2

10. S. W. Davis *et al*., in *Colorado River Origin and Evolution*, R. A. Young, E. E. Spamer, Eds. (Grand Canyon Association, Grand Canyon, AZ, 2001), pp. 135–139.

11. I. Lucchitta, G. H. Curtis, M. E. Davis, S. W. Davis, B. Turrin, Cyclic aggradation and downcutting, fluvial response to volcanic activity, and calibration of soil-carbonate stages in the Western Grand Canyon, Arizona. *Quat. Res.* **53**, 23 (2000). doi:10.1006/qres.1999.2098

12. V. Polyak, C. Hill, Y. Asmerom, Age and evolution of the Grand Canyon revealed by U-Pb dating of water table-type speleothems. *Science* **319**, 1377 (2008). doi:10.1126/science.1151248 Medline

13. J. Pederson, R. Young, I. Lucchitta, L. S. Beard, G. Billingsley, Comment on "Age and evolution of the Grand Canyon revealed by U-Pb dating of water table-type speleotherms". *Science* **321**, 1634b (2008). doi:10.1126/science.1158019

14. R. A. Young, Laramide deformation, erosion and plutonism along the southwestern margin of the Colorado Plateau. *Tectonophysics* **61**, 25 (1979). doi:10.1016/0040-1951(79)90290-7

15. D. P. Elston, R. A. Young, Cretaceous-Eocene (Laramide) landscape development and Oligocene-Pliocene drainage reorganization of Transition Zone and Colorado Plateau, Arizona. *J. Geophys. Res.* **96**, 12389 (1991). [doi:10.1029/90JB01978](doi:10.1029/90JB01978)

16. A. R. Potochnik, in *Colorado River Origin and Evolution*, R. A. Young, E. E. Spamer, Eds. (Grand Canyon Association, Grand Canyon, AZ, 2001), pp. 17–22.

17. R. A. Young, in *Colorado River Origin and Evolution*, R. A. Young, E. E. Spamer, Eds. (Grand Canyon Association, Grand Canyon, AZ, 2001), pp. 7–16.

18. R. A. Young, in *Geology of Grand Canyon, Northern Arizona*, D. P. Elston, G. H. Billingsley, R. A. Young, Eds. (American Geophysical Union, 28th International Geological Congress Fieldtrip Guidebook T115/315, Washington, DC, 1989), pp. 166–173.

19. R. A. Young, in *Late Cenozoic Drainage History of the Southwestern Great Basin and Lower Colorado River Basin: Geologic and Biologic Perspectives*, M. C. Reheis, R. Hershler, D. M. Miller, Eds. (Geological Society of America Special Paper, 2008), vol. 439, pp. 319–333.

20. P. A. Pearthree, J. E. Spencer, J. E. Faulds, P. K. House, Comment on "Age and evolution of the Grand Canyon revealed by U-Pb dating of water table-type speleotherms". *Science* **321**, 1634c (2008). doi:10.1126/science.1158862

21. B. Wernicke, The California River and its role in carving Grand Canyon. *Geol. Soc. Am. Bull.* **123**, 1288 (2011). [doi:10.1130/B30274.1](doi:10.1130/B30274.1)

22. M. A. House, B. P. Wernicke, K. A. Farley, Dating topography of the Sierra Nevada, California, using apatite (U-Th)/He ages. *Nature* **396**, 66 (1998). [doi:10.1038/23926](doi:10.1038/23926)

23. R. M. Flowers, B. P. Wernicke, K. A. Farley, Unroofing, incision and uplift history of the southwestern Colorado Plateau from apatite (U-Th)/He thermochronometry. *Geol. Soc. Am. Bull.* **120**, 571 (2008). [doi:10.1130/B26231.1](doi:10.1130/B26231.1)

24. D. L. Shuster, K. A. Farley, ^{4}He/^{3}He thermochronometry. *Earth Planet. Sci. Lett.* **217**, 1 (2004). [doi:10.1016/S0012-821X(03)00595-8](doi:10.1016/S0012-821X(03)00595-8)

25. K. A. Farley, D. L. Shuster, E. B. Watson, K. H. Wanser, G. Balco, Numerical investigations of apatite ^{4}He/^{3}He thermochronometry. *Geochem. Geophys. Geosyst.* **11**, Q10001 (2010). [doi:10.1029/2010GC003243](doi:10.1029/2010GC003243)

26. K. A. Farley, D. L. Shuster, R. A. Ketcham, U and Th zonation in apatite observed by laser ablation ICPMS, and implications for the (U-Th)/He system. *Geochim. Cosmochim. Acta* **75**, 4515 (2011). [doi:10.1016/j.gca.2011.05.020](doi:10.1016/j.gca.2011.05.020)

27. D. L. Shuster, R. M. Flowers, K. A. Farley, The influence of natural radiation damage on helium diffusion kinetics in apatite. *Earth Planet. Sci. Lett.* **249**, 148 (2006). doi:10.1016/j.epsl.2006.07.028

28. R. M. Flowers, R. A. Ketcham, D. L. Shuster, K. A. Farley, Apatite (U-Th)/He thermochronometry using a radiation damage accumulation and annealing model. *Geochim. Cosmochim. Acta* **73**, 2347 (2009). [doi:10.1016/j.gca.2009.01.015](doi:10.1016/j.gca.2009.01.015)

29. R. M. Flowers, D. L. Shuster, B. P. Wernicke, K. A. Farley, Radiation damage control on apatite (U-Th)/He dates from the Grand Canyon region, Colorado Plateau. *Geology* **35**, 447 (2007). [doi:10.1130/G23471A.1](doi:10.1130/G23471A.1)

30. Materials and methods are available as supplementary materials on *Science* Online.

31. T. A. Dumitru, I. R. Duddy, P. F. Green, Mesozoic-Cenozoic burial, uplift, and erosion history of the west-central Colorado Plateau. *Geology* **22**, 499 (1994). doi:10.1130/0091-7613(1994)022<0499:MCBUAE>2.3.CO;2

32. S. A. Kelley, C. E. Chapin, K. Karlstrom, in *Colorado River Origin and Evolution*, R. A. Young, E. E. Spamer, Eds. (Grand Canyon Association, Grand Canyon, AZ, 2001), pp. 37–42.

33. D. L. Shuster, K. A. Farley, J. M. Sisterson, D. S. Burnett, Quantifying the diffusion kinetics and spatial distribution of radiogenice ^{4}He in minerals containing proton-induced ^{3}He. *Earth Planet. Sci. Lett.* **217**, 19 (2004). [doi:10.1016/S0012-821X(03)00594-6](doi:10.1016/S0012-821X(03)00594-6)

34. K. A. Farley, R. A. Wolf, L. T. Silver, The effects of long alpha-stopping distances on (U-Th)/He ages. *Geochim. Cosmochim. Acta* **60**, 4223 (1996). [doi:10.1016/S0016-7037(96)00193-7](doi:10.1016/S0016-7037(96)00193-7)

35. K. A. Farley, P. W. Reiners, W. Nenow, An apparatus for high-precision helium diffusion measurements from minerals. *Anal. Chem.* **71**, 2059 (1999). [doi:10.1021/ac9813078](doi:10.1021/ac9813078)

36. D. L. Shuster, K. A. Farley, in *Reviews in Mineralogy and Geochemistry: Low-Temperature Thermochronology: Techniques, Interpretations, and Applications*, P. W. Reiners, T. A. Ehlers, Eds. (Mineralogical Society of America, 2005), vol. 58, pp. 181–203.

37. R. A. Ketcham, in *Reviews in Mineralogy and Geochemistry: Low-Temperature Thermochronology: Techniques, Interpretations, and Applications*, P. W. Reiners, T. A. Ehlers, Eds. (Mineralogical Society of America, 2005), vol. 58, pp. 275–314.

38. R. A. Ketcham, R. A. Donelick, M. L. Balestrieri, M. Zattin, Reproducibility of apatite fission-track length data and thermal history reconstruction. *Earth Planet. Sci. Lett.* **284**, 504 (2009). doi:10.1016/j.epsl.2009.05.015

39. J. D. Nations, in *Geology of Arizona*, J. P. Jenny, S. J. Reynolds, Eds. (Arizona Geological Society Digest, Tucson, AZ, 1989), pp. 435–446.

40. J. Zachos, M. Pagani, L. Sloan, E. Thomas, K. Billups, Trends, rhythms, and aberrations in global climate 65 Ma to present. *Science* **292**, 686 (2001). doi:10.1126/science.1059412 Medline